Springer

Journal of Mechanical Science and Technology 22 (2008) 1510~1519

Journal of Mechanical Science and Technology

www.springerlink.com/content/1738-494x
DOI: 10.1007/s12206-008-0609-0

A Method for planar development of 3D surfaces in shoe pattern design

Wanjin Chung[1], Sung-Hwan Kim[2,*] and Ki-Hoon Shin[3]

[1]*Dept. of Die and Mould Engineering, Seoul National University of Technology*
[2]*Dept. of Mechanical Design and Automation Engineering, Seoul National University of Technology*
[3]*Dept. of Mechanical Engineering, Seoul National University of Technology*
172 Gongneung 2-dong, Nowon-gu, Seoul 139-743, Republic of Korea

(Manuscript Received November 12, 2007; Revised May 20, 2008; Accepted June 9, 2008)

Abstract

This paper presents a new method for planar development of the 3D surfaces of a shoe upper. The 3D surface is first faceted into triangular elements and then roughly laid down on a 2D plane. Next, the nodal points of elements are repositioned by a refinement technique that minimizes the geometric errors. Even after elements have been refined by minimizing geometric errors, the resulting 2D shape still has some strain energy that needs to be reduced by a relaxation process. Hence, these elements are then used as an initial guess for further optimization during which the finite element inverse method is used to minimize the total strain energy. In fact, the two-step optimization technique not only can prevent the divergence of solutions (e.g., interferences between elements) but also yields a more reliable result. The method has been implemented as a module of the shoe design system by which a prototype shoe can be designed and manufactured more precisely and quickly.

Keywords: Planar development; Geometric errors; Finite element inverse method; Shoe design system

1. Introduction

CAD systems have been widely introduced in many areas of industry to automate routine procedures, thus increasing speed and consistency while reducing the possibility of mistakes [1]. This is because efficiency and time-to-market are the key factors to success in today's competitive market. In the shoe industry, fashions change rapidly and thus CAD systems are of essence to turn the designer's inspiration into reality quickly, cost-effectively, and accurately.

A shoe mainly consists of an upper and a sole sewn together. The sole, the underside of a shoe, is made of rubber-like resin and produced by injection molding. The upper, everything above the sole, is made by stitching together component pieces, i.e., 2D patterns are first designed on the plain fabric and cut out by dies, and then stitched together to form a 3D shape equivalent to an upper. Traditionally, these component pieces are designed on standard patterns called shells. In fact, a pair of shells, a lateral (outer) shell and a medial (inner) shell, are handmade from a shoe last. Making standard shells from the shoe last, however, is a time-consuming manual process, and thus its accuracy is wholly dependent on the designer's skill. Figs. 1 and 2 show a shoe last and a standard lateral shell manually obtained from a shoe last.

As the demand for design variations increases, the manual process must be automated to enhance the accuracy of the standard shell while providing aesthetically pleasing and functionally comfortable shapes. For this purpose, this paper presents a new method for planar development of the 3D surfaces of a shoe upper to generate more exact 2D standard patterns. We propose a two-step approach combining the geometric error-based method with the finite element inverse method as shown in Fig. 3. A 3D surface is first tessellated into triangular elements and then

*Corresponding author. Tel.: +82 2 970 6344, Fax.: +82 2 974 8270
E-mail address: sunghwan@snut.ac.kr

Fig. 1. A shoe last.

Fig. 2. A standard lateral shell.

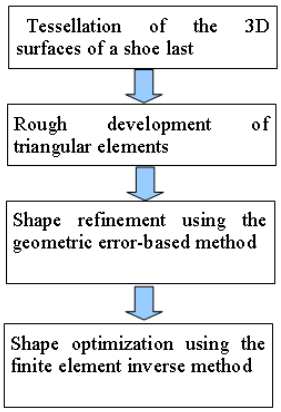

Fig. 3. Overall procedure for planar development of 3D surfaces.

roughly laid down on a 2D plane. Next, the nodal points of elements are iteratively repositioned by a refinement technique that minimizes the geometric errors between the original and the developed elements. Such geometric errors are quantified as changes in the lengths of edges and the areas of elements. Even after elements have been refined by minimizing geometric errors, the resulting 2D shape still has some strain energy that needs to be reduced by a relaxation process. Hence, these elements are then used as an initial guess for further optimization during which the finite element inverse method is used to minimize the total strain energy. In fact, the two-step optimization technique can prevent the divergence of solutions (e.g., interferences between elements) during numerical iterations and thus yields a more reliable result.

2. Related work

Various methods for planar development of 3D sculptured surfaces have been introduced in the clothing, footwear industry, and sheet metal forming. Planar development of cylindrical surfaces and conical surfaces can be done without yielding any distortions such as folds and tears, i.e., these surfaces are developable because their Gaussian curvatures equal zero at all points. However, planar development of spherical surfaces (i.e., non-developable surfaces) always yields some distortions. Even though most sculptured surfaces are non-developable, the elasticity of materials can absorb tensile (or compressive) displacements, thus making them developable within an allowable range of displacement. Therefore, each method specializes in a specific application based on the shapes of surfaces and materials. Methods to develop non-developable surfaces are mainly classified into three categories: geometry-based, decomposition-based, and energy-based methods.

The geometry-based method first tessellates the surface into planar facets and then flattens them by minimizing some geometric properties in the developed patterns. Such geometric properties include the curvature, arc-length, and node angles. Hinds [2] proposed a method for planar development by first approximating the surface with quadrilateral facets, then flattening them allowing some gaps in the developed patterns. Hind's work was improved by Azariadis [3-4] by minimizing the Euclidean distances of pairs of corresponding points between two successive strips. Even though these methods are intuitive, it is difficult to find a globally optimized shape over the working domain because they lack information for error estimation. On the other hand, Maillot et al. [5] proposed a geometric error-based method. Even though this method can yield a reliable result, it has little control over the solution.

The decomposition-based methods [6-8] decompose the curved surface into simpler surfaces and then approximate them with developable surfaces. The lack of continuity along the common edges of adjacent developable surfaces is a drawback of these methods.

The energy-based methods also tessellate the 3D

surface and then map it on a 2D plane. Next, they calculate the difference of the intrinsic energy (e.g., strain-energy) in the original and the mapped elements. The development process then becomes an energy minimization problem. Any solution whose energy level is lower than the predetermined threshold is acceptable. Shimada and Tada [9] proposed a finite element method using the initial guess for stresses on the surface. Some others [10-11] proposed a spring-mass model-based approach where a node is modeled as mass and an edge as spring. On the other hand, the finite element inverse method, based on the ideal forming theory, has been proposed for the design of the initial sheet metal blank [12-14]. This method outputs an initial 2D blank geometry with minimum strain when the final shape of the sheet metal part is pre-defined, thus being called an inverse method. Guo et al. [15] also presented a detailed study on the inverse algorithm and the corresponding implementation procedure with triangular membrane elements. Kim and Huh [16] used this approach in a general multi-step forming with membrane elements. Recently, Yoon et al. [17] applied a direct method, based on the ideal forming theory, for the design of a pre-form in tube hydro-forming. However, the convergence of such methods is not guaranteed with an arbitrary initial guess and thus it may not lead to the closest flattened form for non-developable surfaces. In other words, these methods cannot be properly performed with inverted elements overlapped to each other.

To circumvent a tradeoff between accuracy and stability during planar development, we propose a new method combining the geometric error-based method with the energy-based method using the finite element inverse method. As mentioned earlier, the geometric error-based method is used to yield an initial guess without inverted elements for further optimization that adopts the finite element inverse method.

3. Geometric error-based method

3.1 Rough development

For rough development, a 3D surface is first tessellated into triangular elements. Figs. 4 and 5 show 3D facet models of a toroidal surface and the lateral surface of a shoe last, respectively.

A seed triangle is then chosen approximately at the center of the facet model and arbitrarily laid down on a 2D plane. Next, a triangle that shares an edge with the seed triangle is chosen and flattened while maintaining the original connectivity with the seed triangle. Repeating this step using BFS (Breadth First Search) [18] develops each element one by one. Fig. 6 shows a case in which a triangle is flattened without yielding any overlappings or gaps with adjacent triangles. Fig. 7 shows two cases each of which yields gaps or overlappings, respectively. For these cases, the shapes of two triangles T_1 and T_2 are determined by averaging the coordinates of P_3 and P_3'. Fig. 8 shows the sequence of the rough development.

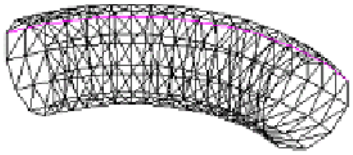

Fig. 4. Facet model of a toroidal surface.

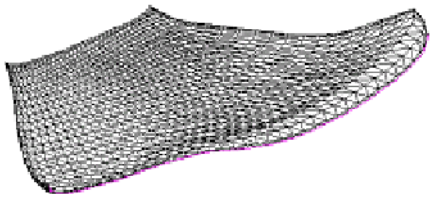

Fig. 5. 3D Facet model of the lateral surface of a shoe last.

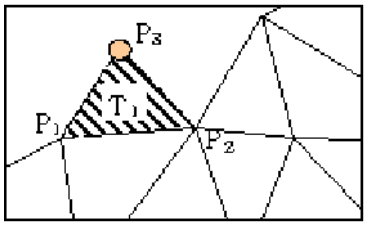

Fig. 6. Mapping of a free triangle.

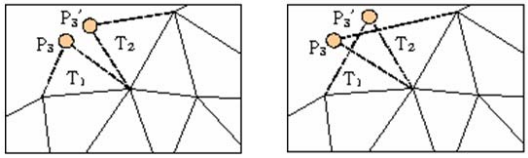

(a) Gaps (b) Overlappings

Fig. 7. Cases yielding gaps or overlappings.

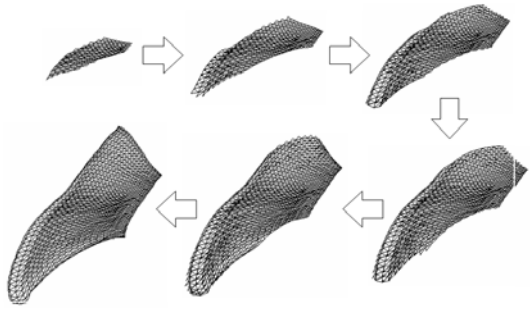

Fig. 8. Sequence of the rough development.

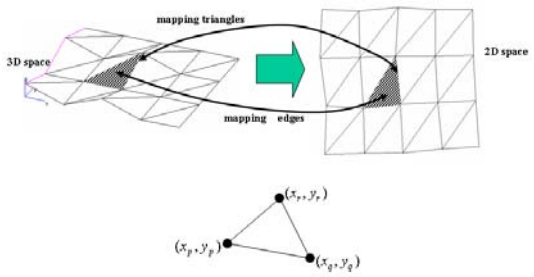

Fig. 9. Planar development.

3.2 Formulation of geometric errors

Fig. 9 shows the planar development from 3D triangular elements to 2D planar elements. Planar development of a non-developable surface always yields some distortions such as folds and tears. Distortions may cause changes in both the lengths of the edges and the areas of the triangular elements. These changes (E_i and T_i) are used to quantify the geometric errors and defined as shown in Eq. (1) and (2). L_{org} and S_{org} denote the length of the edge and the area of the triangular element before development.

$$E_i = (x_p - x_q)^2 + (y_p - y_q)^2 - L_{org}{}^2 \tag{1}$$

$$T_i = (x_q - x_p)(y_r - y_p) - (x_r - x_p)(y_q - y_p) - 2S_{org} \tag{2}$$

Finally, the total geometric error can be formulated by summing the squares of two error terms as shown in Eq. (3). w_e and w_t are weighting factors for the length error and the area error, respectively. n_e and n_t denote the number of edges and triangles in the facet model, respectively.

$$f_{total} = \left(w_e \sum_{i=1}^{n_e} E_i^2 + w_t \sum_{i=2}^{n_t} T_i^2 \right) \tag{3}$$

In particular, the term $(x_q - x_p)(y_r - y_p) - (x_r - x_p)(y_q - y_p)$ in Eq. (2) becomes minus if an element interferes with adjacent elements, thus magnifying the term f_{total}. This property can prevent elements from being inverted and thus improve the convergence of solutions. In fact, the finite element inverse method yields a converged solution only if a sound initial guess without inverted elements is given. This is why a hybrid method is adopted in this paper.

To determine an optimal shape minimizing the total error, we need to optimize the x, y values of all nodal points. The problem of minimizing the total error is over-constrained and thus can be solved by LSM (least squared method) [19]. Constraint equations to be solved by LSM are formulated as follows.

$$f_i = 0, \qquad 1 \le i \le n_e + n_t$$
$$f_i = \begin{cases} E_i & i \le n_e \\ T_{i-n_e+1} & i > n_e \end{cases} \tag{4}$$

The variables to be determined are the x, y values of n nodal points as follows.

$$Q = \{x_1, x_2, ..., x_n, y_1, y_2, ..., y_n\} \tag{5}$$

In addition, we need to define three more equations to prevent the mapped elements from freely moving and rotating on the 2D plane during numerical iterations. In Eq. (6), the first two equations are constraints for coordinates of a node (x_k, y_k) and the third one constrains the rotation of (x_k, y_k) about z axis.

$$\begin{cases} f_{n_e+n_t+1} = x_k - a \\ f_{n_e+n_t+2} = y_k - b \\ f_{n_e+n_t+3} = x_k - x_{k+1} = 0 \end{cases} \tag{6}$$

Once a facet model is generated, the number of unknowns and constraint equations are described as follows.

- Number of unknowns : 2×number of nodes (2 n)
- Number of constraints for length error: n_e
- Number of constraints for area error : n_t
- Number of constraints for Eq. (6): 3

The system above is over-constrained because the number of unknowns ($2n$) is always less than that of constraint equations ($m = n_e + n_t + 3$). The system of equations to be solved by Newton-Raphson method can be formulated as follows.

$$\begin{bmatrix} \frac{\partial f_1}{\partial q_1} & \frac{\partial f_1}{\partial q_2} & \cdots & \frac{\partial f_1}{\partial q_n} \\ \frac{\partial f_2}{\partial q_1} & \frac{\partial f_2}{\partial q_2} & \cdots & \frac{\partial f_2}{\partial q_n} \\ & & \vdots & \\ \frac{\partial f_m}{\partial q_1} & \frac{\partial f_m}{\partial q_2} & \cdots & \frac{\partial f_m}{\partial q_n} \end{bmatrix} \begin{Bmatrix} \Delta q_1 \\ \Delta q_2 \\ \vdots \\ \Delta q_n \end{Bmatrix} = \begin{Bmatrix} -f_1(q_1, q_2, \cdots, q_n) \\ -f_2(q_1, q_2, \cdots, q_n) \\ \vdots \\ -f_m(q_1, q_2, \cdots, q_n) \end{Bmatrix} \tag{7}$$

Eq. (7) can be rewritten to a simple symbolic form as follows.

$$\mathbf{A}_i \cdot \Delta \mathbf{q}_i = -\mathbf{F}(\mathbf{q}_i) \tag{8}$$

The left-hand side ($\mathbf{A}_i$) of the equation is a Jacobian matrix of which the number of rows (m) is greater than that of columns (n). Therefore, there exists no solution because there are more constraints than unknowns, $m > n$. However, if the sum of the squares of the differences between the left and right-hand sides of Eq. (8) is minimized in the least squares sense, the over-constrained linear problem reduces to a solvable linear problem. The reduced set of equations to be solved can be written as the $n \times n$ set of equations by multiplying the transpose of $\mathbf{A}_i$ as follows.

$$\mathbf{A}_i^T \mathbf{A}_i \cdot \Delta \mathbf{q}_i = \mathbf{A}_i^T \cdot -\mathbf{F}(\mathbf{q}_i) \tag{9}$$

Using Newton-Raphson method, the i+1-th solution vector is updated by adding the i-th corrections ($\Delta \mathbf{q}_i$) as follows.

$$\mathbf{q}_{i+1} = \mathbf{q}_i + \Delta \mathbf{q}_i \tag{10}$$

The iteration continues until all components of $\Delta \mathbf{q}_i$ become smaller than a specified tolerance. In fact, the matrix $\mathbf{A}_i^T \mathbf{A}_i$ contains many zero entries (i.e., sparse matrix) and thus we employ the sparse matrix technique [20] to reduce the computing time.

4. Finite element inverse method

Reasonably developed elements could be obtained by the geometric error-based technique mentioned above. However, the resulting 2D shape still has some strain energy since deformation mechanics is not properly considered. It is known that residual strains tend to reduce the service life of shoes. Therefore, we apply the finite element inverse method to minimize the residual strains. Elements refined by geometric error-based method are now used as an initial guess for the subsequent finite element inverse simulation.

In this section, we describe the theory of the finite element inverse method.

When materials are discretized with elements, the plastic work becomes a function of the initial position vector $\mathbf{X}$ and the final position vector $\mathbf{x}$:

$$W = W\left[\bar{\varepsilon}(x_{i=1,2,3}, \mathbf{X}_{i=1,2})\right] = \int \bar{\sigma}(\bar{\varepsilon}) \bar{\varepsilon} dV_0 \tag{11}$$

In Eq. (11), $\bar{\sigma}(\bar{\varepsilon})$, $\bar{\varepsilon}$ and V_0 are the effective stress, the effective strain and the initial volume of the part, respectively. Also, $\mathbf{X}$ and $\mathbf{x}$ are the initial coordinates and the final coordinates in the global Cartesian coordinate systems, respectively. Since V^0 is the volume at the initial (undeformed) configuration, the integration is carried out on the undeformed configuration. For the initial configuration (the embedded material coordinate), the axes 1 and 2 are aligned with the initial flat surface and the axis 3 is perpendicular to the surface as shown in Fig. 10. In general, the plastic work is dependent on the deformation paths of material elements. In the finite element inverse method, the minimum plastic work path is assumed through the total deformation process. In fact, the effective strain is obtained from the flow theory by applying the deformation theory based on the minimum plastic work path [21]. The minimum plastic work path is equivalent to the proportional loading. When the final product shape is prescribed, the plastic work in Eq. (11) becomes a function of $\mathbf{X}$ only.

In order to derive the effective strain $\bar{\varepsilon}$, a material-embedded base vectors for each element is considered at the initial configuration ($t = 0$) as shown in Fig. 10. In this study, linear triangular membrane elements are considered. The deformation gradient can be obtained from the base vectors defined at the initial and final configurations, i.e.,

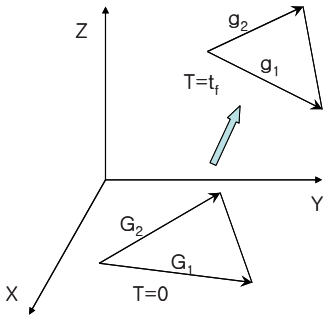

Fig. 10. Material-embedded coordinate system.

$$\mathbf{F} = \mathbf{g}_k \otimes \mathbf{G}^k = (\mathbf{g}_k \cdot \hat{\mathbf{E}}_i)\left(\mathbf{G}_k \cdot \hat{\mathbf{E}}_j\right)^{-1} \hat{\mathbf{E}}_i \otimes \hat{\mathbf{E}}_j,$$
for i=1,2,3, j=1,2, k=1,2 (k is a summation) (12)

where '.' means an inner product. In Eq. (12), g_i and G^i are covariant base vectors of final elements and contravariant base vectors of initial elements for convected coordinate system, respectively. Also, $\hat{\mathbf{E}}_i$ are the base vectors based on the global Cartesian coordinates. Then, the Cauchy strain tensor, $\mathbf{C}(\mathbf{X})$ is

$$\mathbf{C}(\mathbf{X}) = \mathbf{F}^{\mathbf{T}} \cdot \mathbf{F} = C_{ij} \hat{\mathbf{E}}_i \otimes \hat{\mathbf{E}}_j \quad (\text{for } i=1,2, j=1,2) \tag{13}$$

where C_{ij} is the component of the Cauchy strain tensor. The stretch tensor, $\mathbf{U}$ is obtained as follows:

$$\begin{bmatrix} U_{11} & U_{12} \\ U_{21} & U_{22} \end{bmatrix} = \begin{bmatrix} \cos\theta & -\sin\theta \\ \sin\theta & \cos\theta \end{bmatrix} \begin{bmatrix} \sqrt{\lambda_1} & 0 \\ 0 & \sqrt{\lambda_2} \end{bmatrix} \begin{bmatrix} \cos\theta & \sin\theta \\ -\sin\theta & \cos\theta \end{bmatrix}$$
$$= \begin{bmatrix} \sqrt{\lambda_1}\cos^2\theta + \sqrt{\lambda_2}\sin^2\theta & \left(\sqrt{\lambda_1} - \sqrt{\lambda_2}\right)\sin\theta\cos\theta \\ \left(\sqrt{\lambda_1} - \sqrt{\lambda_2}\right)\sin\theta\cos\theta & \sqrt{\lambda_1}\sin^2\theta + \sqrt{\lambda_2}\cos^2\theta \end{bmatrix} \tag{14a}$$

where

$$\begin{bmatrix} \lambda_1 \\ \lambda_2 \\ \theta \end{bmatrix} = \begin{bmatrix} \frac{1}{2}\left(C_{xx} + C_{yy}\right) + \sqrt{\left(\frac{1}{2}\left(C_{xx} - C_{yy}\right)\right)^2 + C_{xy}^2} \\ \frac{1}{2}\left(C_{xx} + C_{yy}\right) - \sqrt{\left(\frac{1}{2}\left(C_{xx} - C_{yy}\right)\right)^2 + C_{xy}^2} \\ \tan^{-1}\left(\frac{C_{xy}}{\lambda_1 - C_{xx}}\right) \end{bmatrix} \tag{14b}$$

$\sqrt{\lambda_i}\,(i=1,2)$ and θ are the principal stretches and the principal direction angle for the Cauchy strain tensor, respectively. Then, the logarithmic strain tensor can be derived as follows:

$$\boldsymbol{\varepsilon}(\mathbf{X}) = \varepsilon_{ij} \hat{\mathbf{E}}_i \otimes \hat{\mathbf{E}}_j = \ln U_{ij} \hat{\mathbf{E}}_i \otimes \hat{\mathbf{E}}_j \tag{15}$$

If the logarithmic strain tensor is given by Eq. (15), the effective strain, $\bar{\varepsilon}$ is a function of $\mathbf{X}$, i.e.,

$$\bar{\varepsilon} = \bar{\varepsilon}(\boldsymbol{\varepsilon}) = \bar{\varepsilon}\left(\boldsymbol{\varepsilon}(\mathbf{X})\right) \tag{16}$$

When the proportional true strain path is imposed, the effective strain can be obtained from the effective strain rate by substituting the rate of deformation tensor $\mathbf{D}^P$ with the true strain tensor, $\boldsymbol{\varepsilon}$, i.e.,

$$\bar{\varepsilon} = \bar{\varepsilon}(\boldsymbol{\varepsilon}) \Leftrightarrow \dot{\bar{\varepsilon}} = \dot{\bar{\varepsilon}}(\dot{\boldsymbol{\varepsilon}}) \tag{17}$$

In this work, a rate-independent isotropic rigid-plastic material is considered. Thus, the quadratic strain rate potential suggested by Hill et al. [22] could be integrated to the following form.

$$\begin{bmatrix} \sigma_{xx} \\ \sigma_{yy} \\ \sigma_{xy} \end{bmatrix} = \frac{2\bar{\sigma}}{3\bar{\varepsilon}} \begin{bmatrix} 2 & 1 & 0 \\ 1 & 2 & 0 \\ 0 & 0 & 1 \end{bmatrix} \begin{bmatrix} \varepsilon_{xx} \\ \varepsilon_{yy} \\ \varepsilon_{xy} \end{bmatrix} \tag{18}$$

where $\bar{\varepsilon}$ and $\bar{\sigma}$ are the total equivalent strain and equivalent stress. Initial configuration can be obtained by applying the condition of minimum plastic work:

$$\frac{\partial W}{\partial \mathbf{X}} = 0 \tag{19}$$

where $X_{i=1,2}$ is contained on the initial flat blank. In Eq. (19), therefore, all material elements are prescribed to stay on the surface of the initial blank sheet, while the plastic work is optimized with respect to the two components of each nodal point, not to all three components of the position vector. In order to solve Eq. (19) with a Newton–Raphson solver, the following linearization is performed.

$$\frac{\partial^2 W(\mathbf{X})}{\partial \mathbf{X} \partial \mathbf{X}} \delta \mathbf{X} = -\frac{\partial W(\mathbf{X})}{\partial \mathbf{X}} \quad , \tag{20}$$

5. Case study

As a module of an integrated shoe design system, we implement the proposed method for planar development of 3D sculptured surfaces. Actual implementation is done in C++ and Unigraphics using UG/Open. This section presents the developed results of two shells (a lateral shell and a medial shell), which are respectively computed from two 3D surfaces that form the upper of a left shoe last.

5.1 Minimization of geometric errors

Two 3D surfaces, which form the upper of a

shoe last, are first tessellated into triangular elements and then roughly laid down on a 2D plane

Table 1. Iteration result.

Iteration	Error sum	Max (Δq_i)	Time (sec)
1	12796.39	12.1574	1.016
2	8305.10	1.7431	2.078
3	8300.23	0.0817	3.156
4	8300.06	0.0163	4.235
5	8300.03	0.0096	5.360
6	8300.02	0.0082	6.469
7	8300.01	0.0043	7.563
8	8300.01	0.0026	8.625
9	8300.00	0.0015	9.688
10	8300.00	0.0016	11.000

by BFS algorithm. Next, these elements are refined by the geometric error-based method proposed in section 3. In fact, 924 nodes and 1,722 triangular elements are used to approximate each 3D surface.

Table 1 presents the test result in which the error sum shown in Eq. (3), the maximum correction (Max $\Delta \mathbf{q}_i$), and the computing time are shown with respect to the number of iterations. According to the result, the error sum rapidly converges and thus hardly changes after three iterations. The maximum correction becomes smaller than 0.01 after five iterations. The time is measured on a Pentium (Sonoma) computer with 2.13 GHz CPU.

5.2 Minimization of the total strain energy

5.2.1 Evaluation of material properties

To obtain the material properties required for finite element simulation, the tensile test of a leather sheet is first carried out according to the standard test procedure. Tensile test is performed along two orthogonal directions with the ram speed of 1mm/s. Fig. 11 shows stress-strain curves measured up to the strain of 0.3 in two orthogonal directions. Thus, it can be said that the test is performed sufficiently above the maximum strain, usually less than 0.2, occurred in the real development. Material properties along two orthogonal directions do not reveal much difference. Therefore, for simplicity, we assume that the material is isotropic and rigid-plastic. The mean stress-strain relationship is given in the form of a table in the analysis.

5.2.2 Results

Using the elements refined by the geometric error-based method as an initial guess, the finite element inverse method yields an optimal shape with minimum strain as mentioned earlier. Table 2 presents the

Table 2. Iteration result by finite element inverse method.

Iteration	Max (Δq_i)
1	14.0981
2	2.6060
3	7.4732
4	0.3861
5	0.2668
6	0.0127
7	0.0010
8	0.0001

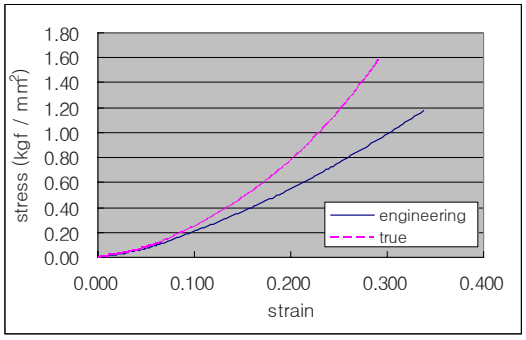

(a) First direction

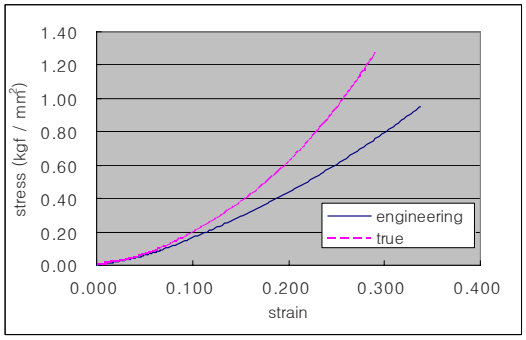

(b) Second direction

Fig. 11. Stress-strain curves of a leather sheet along two orthogonal directions.

test result in which the maximum correction (Max $\Delta \mathbf{q}_i$) is listed according to the iteration number. The total computing time is 4.68sec with 8 iterations using a Pentium (Sonoma) computer with 2.13 GHz CPU. According to the result, the maximum correction rapidly converges and falls under 0.001 after seven iterations.

Figs. 12- (a) and (b) show the effective strain distributions on the inner (medial) side and the outer

(lateral) side, both of which together form the upper of a left shoe. In Fig. 12- (a), a maximum strain is

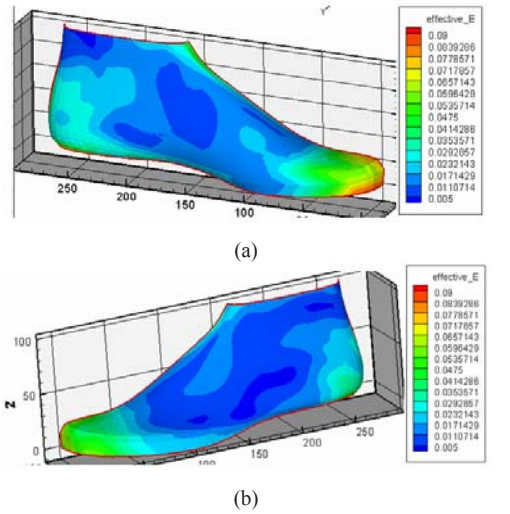

Fig. 12. Effective strain on (a) the inner (medial) side and (b) the outer (lateral) side of a left shoe after the finite element inverse analysis.

found around the big toe and relatively high strains are also observed in the neighborhood of the heel. Fig. 13 shows the effective strain distributions plotted on the initial 2D blank of the inner side for the convenience of visualization. After the finite element inverse method, relatively high strains around the big toe are substantially reduced as shown in Fig. 13- (b). Fig. 13 (c) shows the difference of the effective strains before and after the finite element inverse analysis shown in Fig. 13- (a) and (b), respectively. It is clearly shown that strains are considerably reduced in Fig. 13- (c).

Fig. 14 shows the effective strain distributions with respect to the element number. The maximum strain decreases below 0.11 after the analysis while the maximum effective strain reaches up to around 0.17 before the analysis. Even though the effective strains of some elements increase a little bit, those of most elements decrease on the whole. Fig. 15 shows the effective strain distributions on the outer (lateral) side. Although the finite element inverse method also reduces the strain distribution effectively on the outer side, the reduction of the effective strain is smaller than that on the inner side as shown in Figs. 14- (c) and 15- (c).

Fig. 16 shows handmade shells overlapped by resulting shapes obtained by the finite element analysis. Two handmade shells are denoted by thick lines and the resulting shapes are denoted by thin circled lines. In each case, the handmade shell is compared with the resulting shape by referencing two curves, denoted by

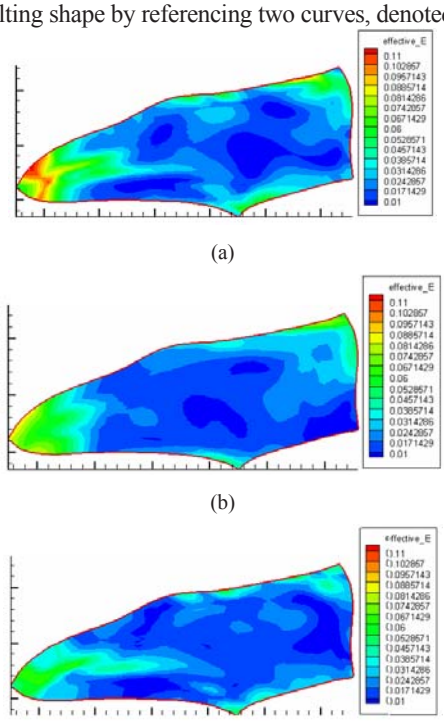

Fig. 13. On the inner side, (a) effective strain before (a) effective strain after the finite element inverse analysis, (c) difference of effective strains before and after the analysis, plotted on the initial 2D blank.

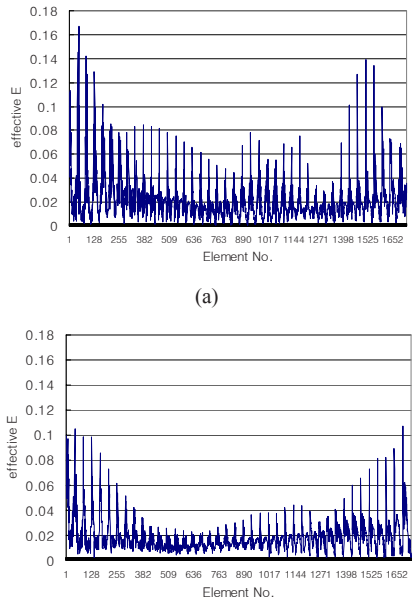

Fig. 14. On the inner side, (a) effective strain before, (b) effective strain after the finite element inverse analysis.

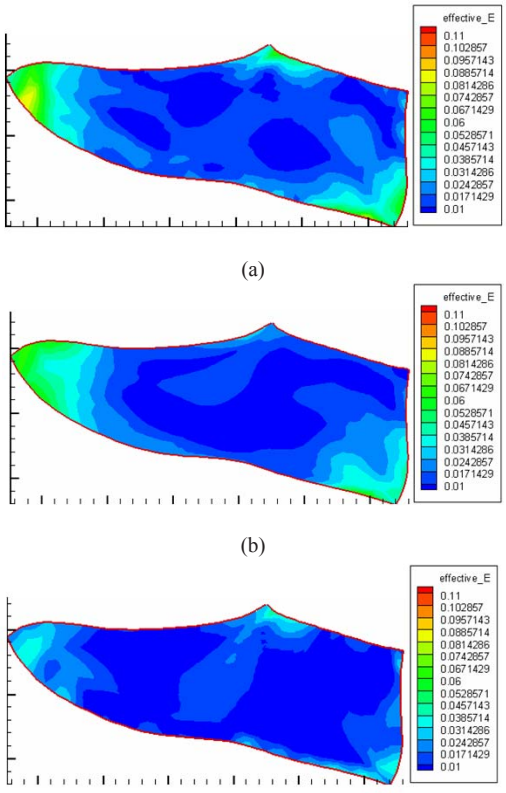

(a)

(b)

(c)

Fig. 15. On the outer side, (a) effective strain before, (a) effective strain after the finite element inverse analysis, (c) difference of effective strains before and after the analysis, plotted on the initial 2D blank.

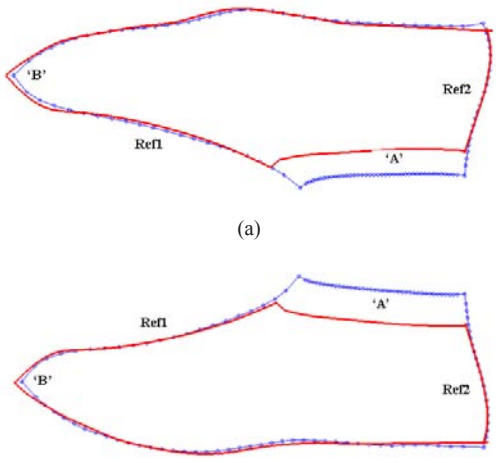

(a)

(b)

Fig. 16. Comparison between handmade shells and resulting shapes after the finite element inverse analysis on (a) the inner (medial) side and (b) the outer (lateral) side.

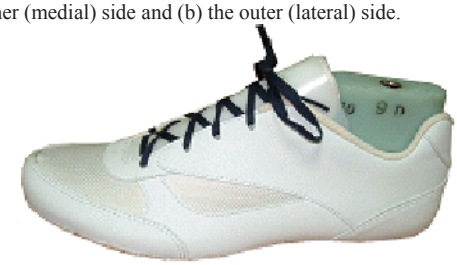

Fig. 17. A prototype shoe.

ref1 (instep curve) and ref2 (heel curve). The mismatches nearby the ankle, marked by 'A', are not important because they are originated from the difference between two CAD models; one is obtained from the 3D surface of a shoe last and the other is digitized from the handmade shell. On the whole, the resulting shapes match well with the handmade shells except for the tiptoe marked by 'B'. According to the actual test, the resulting shapes prove to be in close agreement with the experience of the skilled designer. Fig. 17 shows a prototype shoe, which was produced using two standard shells obtained by the proposed method.

6. Conclusions

This paper presents a new method for planar development of 3D surfaces of a shoe last to generate more exact 2D standard patterns. We propose a two-step approach combining the geometric error-based method with the finite element inverse method. The 3D surface is first tessellated into triangular elements and then roughly laid down on a 2D plane. Next, the nodal points of elements are iteratively repositioned by a refinement technique that minimizes the geometric errors between the original and the developed elements. Such geometric errors are quantified as changes in the lengths of edges and the areas of elements. Even after elements have been refined by minimizing geometric errors, the resulting 2D shape still has some strain energy, which needs to be reduced by a relaxation process. Hence, these elements are then used as an initial guess for further optimization during which the finite element inverse method is used to minimize the total strain energy. In fact, the two-step optimization technique can prevent the divergence of solutions (e.g., interferences between elements) during numerical iterations and thus yields

a more reliable result. The proposed method is implemented in Unigraphics using UG/Open and applied to the actual shoe pattern design. The examples validate the efficiency and usefulness of the proposed method.

References

[1] K. Lee, Principles of CAD/CAM/CAE Systems, Addison Wesley, (1999).

[2] B. K. Hinds, J. McCartney and G. Woods, Pattern development for 3D surfaces, *Computer Aided Design* 23 (8) (1991) 583-592.

[3] P. Azariadis and N. Aspragathos, Design of plane developments of doubly curved surfaces, *Computer Aided Design* 29 (10) (1997) 675-685.

[4] P. Azariadis, A. Nearchou and N. Aspragathos, An evolutionary algorithm for generating planar developments of arbitrarily curved surfaces, *Computers in Industry* 47 (3) (2002) 357-368.

[5] J. Maillot, H. Yashia and A. Verroust, Interactive texture mapping, *Proc SIGGRAPH 93*, Anaheim, CA, USA, (1993) 27-34.

[6] G. Elber, Model fabrication using surface layout projection, *Computer Aided Design* 27 (4) (1995) 283-291.

[7] J. Hoschek, Approximation of surfaces of revolution by developable surfaces, *Computer Aided Design* 30 (10) (1998) 757-763.

[8] R. M. C. Bodduluri and B. Ravani, Design of developable surfaces using duality between plane and point geometries, *Computer Aided Design* 25 (10) (1993) 621-632.

[9] T. Shimada and Y. Tada, Approximate transformation of an arbitrary curved surface into a plane using dynamic programming, *Computer Aided Design* 23 (2) (1991) 153-159.

[10] J. Fan , Q. Wang, S. Chen, M. Yuen and C. Chan, A Spring-Mass Model-Based Approach for Warping Cloth Patterns on 3D Objects, *Journal of Visualization and Computer Animation* 9 (4) (1998) 215-227.

[11] C. Wang, S. Smith and M. Yuen, Surface flattening based on energy model, *Computer Aided Design* 34 (2002) 823-833.

[12] K. Chung and O. Richmond, Ideal forming, part I: homogeneous deformation with minimum plastic work, *International Journal of Mechanical Sciences* 34 (1992) 575–591.

[13] K. Chung and O. Richmond, Ideal forming, part II: sheet forming with optimum deformation, *International Journal of the Mechanical Sciences* 34 (1992) 617-633.

[14] K. Chung, J. W. Yoon and O. Richmond, Ideal sheet forming with frictional constraints, *International Journal of Plasticity* 16 (2000) 595–610.

[15] Y. Q. Guo, J. L. Batoz and J. M. Duroux, Finite element procedures for strain estimation of sheet metal forming parts, *International Journal for Numerical Methods in Engineering* (8) (1990) 1385-1401.

[16] S. H. Kim and H. Hub H., Finite element inverse analysis for the design of intermediate dies in multistage deep drawing processes with large aspect ratio, *Journal of Materials Processing Technology* 113 (2001) 779-785.

[17] J. W. Yoon, K. Chung, F. Pourboghrat and F. Barlat, Design optimization of extruded perform for hydroforming processes based on ideal forming design theory, *International Journal of Mechanical Sciences* 48 (2006) 1416–1428.

[18] E. Horowitz and S. Sahni, *Fundamentals of Data Structure*, Computer Science Press, (1983).

[19] J. D. Faires and R. L. Burden , *Numerical Methods*, International Thomson Publishing, (1996).

[20] K. S. Kundert and V. Sangiovanni, *A Sparse User's Guide A Sparse Linear Equation Solver*, Dept. of Electrical Engineering and Computer Sciences, U.C. Berkeley, (1998).

[21] K. Chung, and O. O. Richmond, A deformation theory of plasticity based on minimum work paths, *International Journal of Plasticity* 9 (1993) 907–920.

[22] R. Hill, The Mathematical theory of plasticity, Clarendon Press, (1950).